

## ORIENTATION OF THE MAGNETIC FIELDS IN INTERPLANETARY FLUX ROPES AND SOLAR FILAMENTS

VASYL B. YURCHYSHYN,<sup>1,2</sup> HAIMIN WANG,<sup>1</sup> PHILIP R. GOODE,<sup>1</sup> AND YUANYONG DENG<sup>3</sup>

Received 2001 June 4; accepted 2001 August 10

### ABSTRACT

Coronal mass ejections (CMEs) are often associated with erupting magnetic structures or disappearing filaments. The majority of CMEs headed directly toward the Earth are observed at 1 AU as magnetic clouds—the region in the solar wind where the magnetic field strength is higher than average and there is a smooth rotation of the magnetic field vectors. The three-dimensional structure of magnetic clouds can be represented by a force-free flux rope. When CMEs reach the Earth, they may or may not cause magnetic storms, alter Earth's magnetic field, or produce the phenomena known as auroras. The geoeffectiveness of a solar CME depends on the orientation of the magnetic field in it.

Two M-class solar flares erupted on 2000 February 17. The second flare occurred near a small active region, NOAA Active Region 8872. This eruption was accompanied by a halo CME. However, the February 17 CME did not trigger any magnetic activity when it arrived at the Earth. Another powerful flare, on 2000 July 14, was also associated with a halo CME, which caused the strongest geomagnetic activity of solar cycle 23. Using *ACE* measurements of the interplanetary magnetic fields, we study the orientation of the magnetic flux ropes in both sets of magnetic clouds and compare them with the orientation of the solar magnetic fields and disappearing filaments. We find that the direction of the axial field and helicity of the flux ropes are consistent with those of the erupted filaments. Thus, the geoeffectiveness of a CME is defined by the orientation and structure of the erupted filament and by its magnetic helicity as well. We also suggest that the geoeffectiveness of a CME can be forecasted using daily full-disk  $H\alpha$  and *Yohkoh* images and MDI magnetograms as well.

*Subject headings:* Sun: coronal mass ejections (CMEs) — Sun: magnetic fields

### 1. INTRODUCTION

The coronal transients involving the ejection of plasma and magnetic fields from the Sun are referred as coronal mass ejections (CMEs). They represent a large-scale rearrangement of the solar magnetic fields and can lead to a significant disturbance of the Earth's magnetic field. Each CME may carry away a mass of up to  $10^{13}$  kg and release up to  $10^{25}$  J of energy from coronal magnetic fields (see Chen 2001 for a review). Following their discovery, CMEs were soon found to be correlated with the occurrence of geomagnetic storms (Burlaga et al. 1981; Wilson & Hildner 1984). Bothmer & Schwenn (1994) and Rust (1994) showed that filament chirality and the orientation of filament magnetic fields correspond to the chirality and orientation of the magnetic fields in magnetic clouds. McAllister & Martin (2000) studied the role reconnection may play in the eruption process. They found that, if reconnection is involved in the eruption process, the topology of a magnetic cloud can be predicted from the preeruption filament and posteruption coronal arcade. On the other hand, observations suggest that the magnetic fields are already twisted when they emerge (Tanaka 1991; Leka et al. 1996), and a flux rope can form long before eruption (Matsumoto et al. 1993; Rust 1994).

Establishing the correlation among the occurrence of CMEs and other solar surface phenomena, such as filament eruptions, flares, or preflare topology of the magnetic fields,

just to name few, is a long-standing problem in solar physics. CMEs are easily observed at the solar limb, where they are seen against a dark background. However, the Earth-directed, disk CMEs are much harder to detect, although they are the ones that have the most important geomagnetic effects. Therefore, detecting the early manifestation of CMEs on the solar disk is essential to understanding Earth-directed CMEs themselves. From *Yohkoh* images, Canfield, Hudson, & McKenzie (1999) have found that active regions with an X-ray sigmoid structure are more likely to produce a flare-associated CME. However, only those CMEs with magnetic fields having a southward component are capable of producing large geomagnetic storms (Chen 2001).

The goal of this work is to combine high-quality observations of the solar surface and of interplanetary space to better understand the relations between magnetic structures in CME source regions and magnetic clouds. To do this, we will compare observations of two solar disk flares with disturbances (in the form of magnetic clouds) observed by *ACE*.

### 2. DATA

We used the global  $H\alpha$  network observations. The data are Big Bear Solar Observatory (BBSO) and Huairou Solar Observing Station (HSOS) full-disk  $H\alpha$  images. The time cadence was 1 minute and the pixel resolution was  $1''$ . HSOS (pixel size  $0''.6$ ) and full-disk MDI (pixel size  $2''$ ) longitudinal magnetograms were used to study the magnetic field distribution and to extrapolate the observed field into the corona. The modeled force-free field was compared with *Yohkoh* soft X-ray data, with a pixel resolution of  $4''.92$ , and *TRACE* data (only for the 2000 July 14 solar flare). We also

<sup>1</sup> Big Bear Solar Observatory, Big Bear City, CA 92314.

<sup>2</sup> Crimean Astrophysical Observatory, 98409 Nauchny, Crimea, Ukraine.

<sup>3</sup> Beijing Astronomical Observatory/National Astronomical Observatories, Chinese Academy of Sciences, 20 Datun Road, Chaoyang, Beijing 100012, China.

used the C2 and C3 white-light LASCO data, which cover the range from 2 to 32 solar radii.

*ACE* one-hour averages of magnetometer data were used to study the structure of the interplanetary magnetic field. The satellite orbits the Sun at about 1.5 million km from the Earth, giving approximately 1 hr advance warning of geomagnetic storms.

Because most of the data used are full-disk images, the alignments were straightforward. We found the center of radius of each image by limb fitting and made a rotational adjustment by visual inspection. Then, the *TRACE* high-resolution white-light and Fe XII 195 Å images were aligned with the full-disk white-light image and MDI magnetogram. The HSOS high-resolution magnetogram was aligned with the MDI magnetogram.

### 3. DETERMINATION OF THE HELICITY SIGN IN AN ACTIVE REGION

The sign of the magnetic helicity can be determined by several different means. In the solar atmosphere, magnetic helicity and current helicity have the same sign (Seehafer 1990); hence, direct calculation of current helicity (Seehafer 1990; Pevtsov, Canfield, & Metcalf 1995; Abramenko, Wang, & Yurchishin 1996) is the most reliable method. However, it requires vector magnetic field data, which are not available for the active regions under study.

In the higher levels of the solar atmosphere, under normal circumstances the magnetic field often dominates the solar plasma. The solar plasma, seen in chromospheric and coronal images, is structured by the magnetic fields, and these plasma structures indicate magnetic lines of force (Smith 1968). It has also been found that global patterns of helicity, or handedness, are present in Sun's magnetic fields, and they are associated with plasma structures (Rust 1994; Zirker et al. 1997). Solar spots (Hale 1927; Richardson 1941), active region fields (Seehafer 1990; Pevtsov et al. 1995; Abramenko et al. 1996), X-ray loops (Webb 1992; Rust & Kumar 1996; Canfield et al. 1999), and chromospheric filaments and fibrils (Martin, Billimoria, & Tracadas 1994) exhibit such helicity patterns. Thus, the sign of the magnetic helicity can also be derived using chromospheric ( $H\alpha$ ) and coronal (*Yohkoh*, *TRACE*) images.

*X-ray Sigmoids*.—The association between S-shaped sigmoids and magnetic fields having positive and negative helicity was developed by Nakagawa et al. (1971). Rust & Kumar (1996) concluded that the helicity segregation, established for magnetic flux ropes, also holds for bright coronal X-ray sigmoid structures. Reverse-S sigmoids (negative helicity) predominate in the northern hemisphere, while forward-S sigmoids (positive helicity) predominate in the southern hemisphere.

*Dextral and sinistral filaments*.—Analyses of  $H\alpha$  filaments and photospheric magnetograms have revealed two chiralities of filaments, dextral and sinistral (Martin et al. 1994). If a filament's axial field is directed rightward (leftward), when viewed by an observer at the positive-polarity side of the filament, then the filament is called dextral (sinistral). Rust & Martin (1994) found a one-to-one relationship between counterclockwise (clockwise) whorls and dextral (sinistral) filaments, which strongly suggests that dextral (sinistral) filaments contain negative (positive) helicity fields. It also is accepted that chromospheric fibrils form a spiral around a sunspot and are twisted counterclockwise (clockwise) if the sunspot rotates in that direction. Rust & Martin (1994) also

found that an active region filament with an end curving toward a sunspot with counterclockwise (clockwise) twist is dextral (sinistral).

*Magnetic field modeling*.—Observed  $H\alpha$  and/or EUV structures can be compared with magnetic field lines as calculated from a magnetogram. From such a comparison of field line connectivity and orientation, we can determine the sign of magnetic helicity. This method is very reliable in the case of magnetically complex active regions.

## 4. RESULTS

### 4.1. Halo CME on 2000 February 17

Figure 1 shows BBSO  $H\alpha$  images of a 2000 February 17 flare in NOAA Active Region 8872 at S29 E07. The active region showed very little activity before the flare. In the preflare image at 20:06:39 UT, one can see that side-by-side filaments are simultaneously present in the active region. They are marked "A" and "D." The flare started at about 20:05 UT, in the form of small, bright  $H\alpha$  patches along filament D. By 20:15:39 UT, the filament had already disappeared. In the subsequent panels, its former position is marked with a segment of a thick black line. The MDI image at 17:35:00 UT (*top right*) shows that filament A overlies the neutral line, while filament D overlies an extended magnetic area of positive polarity. The bottom panels of the figure show the further evolution of the flare and modeled magnetic field above the active region. The flare evolved as a typical two-ribbon flare. Interesting to note, we still can see filament A between the flare ribbons throughout the flare (20:48:39 UT image).

The linear force-free field extrapolation (Abramenko & Yurchishin 1996) shows that the magnetic field in the active region can be fitted by a linear model with positive parameter  $\alpha = 0.010 \text{ arcsec}^{-1}$  (positive helicity). The orientation of simulated field lines matches both the chromospheric structures and the sigmoid observed by *Yohkoh* (Figs. 1 and 2). Orientation of chromospheric fibrils and calculated field lines (Figure 1) form a spiral, which would result when a solar spot rotated in the clockwise direction. The forward-S sigmoid (Fig. 2) also suggests that the active region has positive magnetic helicity.

The flare gave rise to a halo CME observed by LASCO on board *SOHO* (Fig. 3). The halo CME was expected to trigger aurora and other geomagnetic activity when it passed by our planet around February 20. Figure 4 is a plot of 1 hr averages of the interplanetary magnetic field (IMF) at about 0.99 AU. We identify a magnetic cloud (MC) as follows (Klein & Burlaga 1982): (1) rotation of the magnetic field, (2) magnetic field strength higher than 10 nT, (3) structure duration of more than 1 day. According to *ACE* measurements, the CME reached the Earth's magnetosphere on February 21; however, there were no signs of geomagnetic activity following the CME. The bottom panel in Figure 4 shows the variations of the Dst index<sup>4</sup> between 03:30 UT February 21 and 15:30 UT February 22. The plot shows fairly small fluctuations in the Dst index during the passage of the MC (note that a geomagnetic storm begins when the Dst index drops below  $-60$ ).

From Figure 4 (*X-Z* plot) we see that the  $B_z$  component of the IMF was directed mostly northward and did not

<sup>4</sup> The Dst index is an index of magnetic activity derived from near-equatorial geomagnetic measurements of the intensity of the globally symmetrical equatorial electrojet (the "ring current").

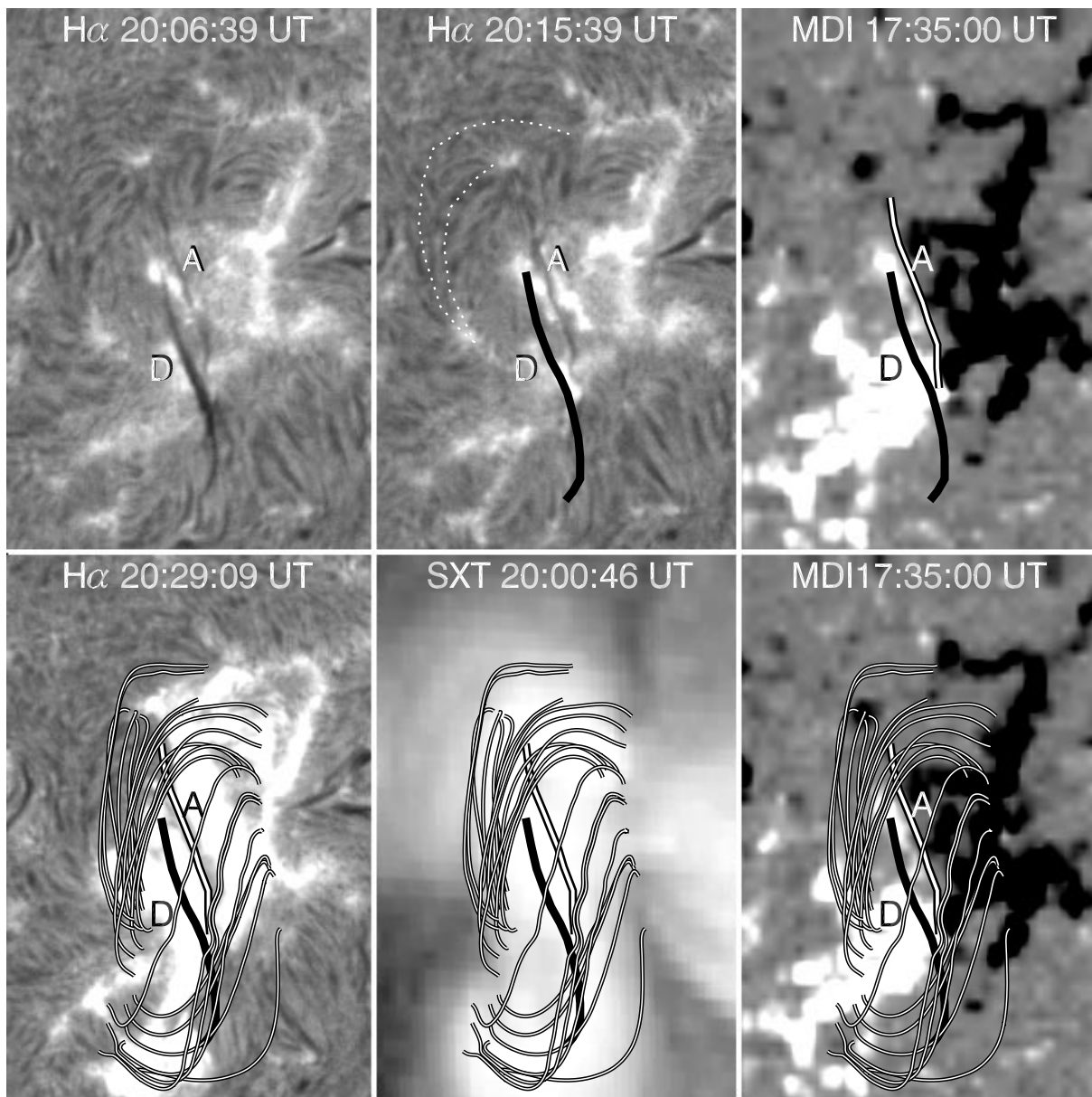


FIG. 1.—BBSO  $H\alpha$  *Yohkoh*/SXT and MDI magnetic field observations of a 2000 February 17 two-ribbon flare. Bottom panels are overlaid with linear force-free field lines ( $\alpha = 0.01 \text{ arcsec}^{-1}$ ). MDI magnetogram shows positive ( $N$ ) fields in white, negative ( $S$ ) fields in black. The dotted lines in the  $H\alpha$  20:15:39 UT images show approximate direction of the horizontal magnetic field as derived using chromospheric dark filaments. Filament D disappeared, and its former position is denoted by the black solid line. North is to the top, west is to the right.

change sign during the passage of the satellite through the MC. The same is true of the  $B_x$  component, which was directed earthward ( $X$ - $Y$  plot). The only component that changes sign is  $B_y$  ( $X$ - $Y$  and  $Y$ - $Z$  plots). Burlaga (1988) showed that many MCs can be modeled by a force-free magnetic flux rope. From Figures 4 and 5, it is possible to find the orientation of the flux rope. The fact that the  $B_y$  component has changed sign implies that it is the azimuthal component of the flux rope's magnetic field and that the axis of the flux rope was oriented vertically, i.e., in the south-north direction. If the flux rope were oriented in the east-west direction, then we would see the rotation of the  $B_z$  component.  $B_y$  vanishes on February 22 at about  $t_2 = 00:00$  UT. This means that the axis of the flux tube lies nearly in the  $X$ - $Z$  plane of the GSE system, i.e., approximately along the projection of Sun's north-south axis;

otherwise, the  $B_y$  component would not vanish (note that, on February 14,  $P_0 = -18^\circ$ ).

Because filament D disappeared in the course of the flare, a possible explanation of the origin of the February 17 CME is a filament eruption. However, during the disappearance the filament faded in  $H\alpha$  while being stationary, with its general shape remaining the same. These are signatures of thermal sudden disappearance due to an increase in the energy input, leading to ionization of the hydrogen (Mouradian, Soru-Escout, & Pojoga 1995). It is also known that thermal disappearance produces no CMEs. It seems unlikely that a preexisting flux rope (filament D) erupted, originating the CME. The fact that the  $H\alpha$  flare started about 10 minutes before the filament disappearance favors this suggestion, because the flare could supply the energy necessary to heat the filament. At the same time, it also

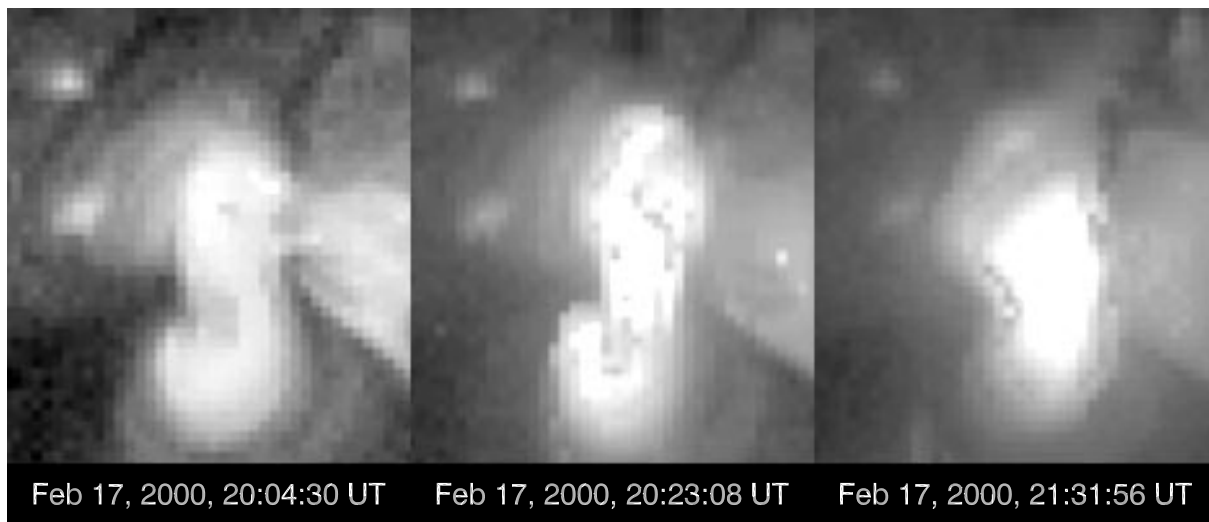


FIG. 2.—*Yohkoh* image at 20:04:30 UT, showing a preflare sigmoid that resides in the middle of the active region. After flare onset, at 20:23:08 UT, the sigmoid has changed and its brightness has increased. By the end of the flare, the sigmoid is no longer seen and a system of bright postflare loops forms. North is to the top, west is to the right.

offers another way to explain the origin of the CME. It has been suggested (Gosling 1993; Chen 2001) that if the initial structure before the CME onset were an arcade it must undergo reconnection to form a flux rope and thus a solar flare precedes the eruption. There are two sets of highly sheared magnetic fluxes that can be identified in *Yohkoh* images, connecting different parts of the active region and forming the upper and lower parts of the sigmoid structure (see Fig. 2). Amari et al. (2000) showed that a highly sheared magnetic configuration may produce a twisted magnetic flux rope, which is unstable and erupts. In this configuration, the axial field in the newly formed large-scale flux rope would be northward-directed, and the flux rope possesses a positive magnetic helicity, which agrees with the *ACE* measurements (Fig. 4). This configuration may also account for the origin of the February 17 CME and of the two-ribbon flare as well. The trigger of the reconnection may be continuous photospheric motion (Amari et al. 2000) or a propagating disturbance from another flare in the neighboring active region (Wang et al. 2001).

4.2. Halo CME on 2000 July 14

One of the largest and most powerful events of solar cycle 23 flared in NOAA AR 9077 on 2000 July 14. The flare started as small, bright patches along the line of the dark

filament, long before the filament eruption (Fig. 6). A detailed and comprehensive description of the event is given in Zhang et al. (2001). According to the authors, the trigger of the flare was magnetic flux cancellations at many sites in the vicinity of the filament. Kosovichev & Zharkova (2001) also reported rapid oscillations in the magnetic field during the flare. The *Yohkoh* image at 09:27 UT (Fig. 7, top left panel) shows a large preflare X-ray loop, which spanned the entire active region. The loop is not visible in the *TRACE* Fe XII 195 Å image and apparently represents a high coronal structure. We cannot exclude the possibility that

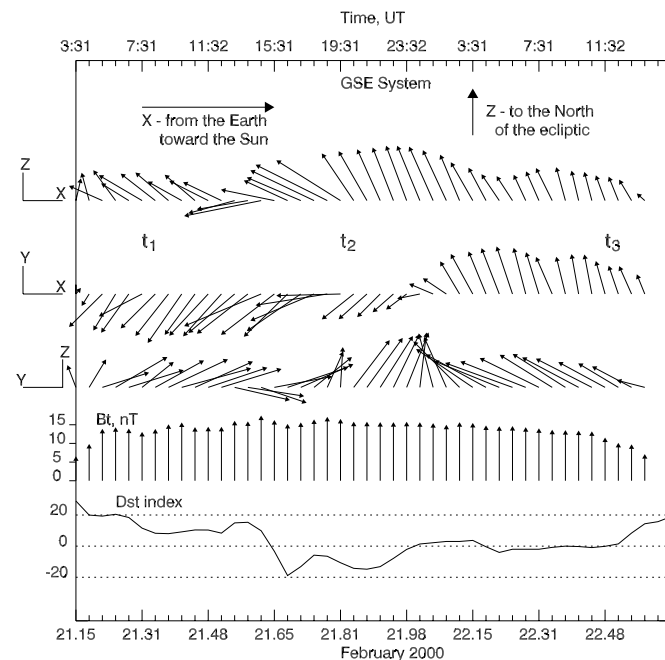


FIG. 4.—One-hour averages of the IMF in an MC at about 0.99 AU (near the Lagrange point L1). Magnetic field components are plotted in the GSE system, where the X-axis points from the Earth toward the Sun, Y is in the ecliptic plane and negative in the direction of planetary motion, and Z is parallel to the ecliptic pole. Two bottom panels show variations of the IMF strength and the Dst index.

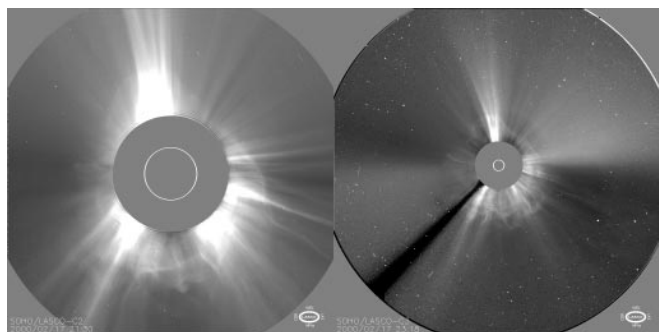


FIG. 3.—LASCO C2 at 21:39 UT (left) and LASCO C3 at 23:18 UT (right) images showing a halo CME on 2000 February 17.

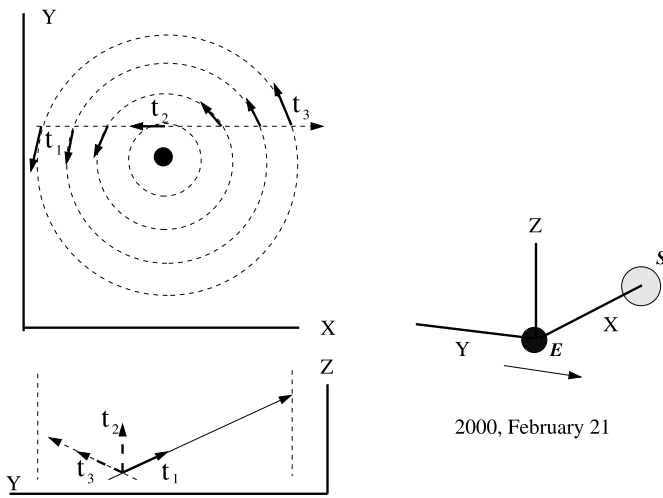


FIG. 5.—Cartoon showing the orientation of the flux rope in the February 21 MC. Coordinate system is GSE.

this large X-ray structure is a superposition of several sheared arches; however, for sake of simplicity, we will refer to it as a large X-ray loop.

The eruption started approximately at 09:30 UT by the activation of a low-lying dark filament visible in the *TRACE* and  $H\alpha$  images, as indicated by the arrow in

Figure 7 (see also Zhang et al. 2001). Presumably, the filament eruption led to the destabilization of the large X-ray loop: the top right image in Figure 7 shows the postflare magnetic configuration, where the X-ray loop is no longer seen. Instead, in the 01:01 UT *Yohkoh* and 10:33 UT *TRACE* images, there is a long-lasting postflare loop system.

Two bottom panels in Figure 7 show the HSOS magnetogram taken several hours before the flare and a linear force-free field with  $\alpha = -0.019 \text{ arcsec}^{-1}$ . Because of the limitations of a linear force-free model, we failed to reproduce the observed large-scale coronal field in detail. A comparison of the calculated field lines with the 09:27 UT *Yohkoh* image shows that the observed field is far more twisted than the modeled field. Normally,  $|\alpha| \leq 0.02 \text{ arcsec}^{-1}$  is enough to fit the large-scale field of an active region. On the other hand, the model with negative helicity matches the postflare loop system seen in the 10:33 UT *TRACE* image.<sup>5</sup> When we look at the observed postflare loop system from the positive-polarity side, we find that the magnetic field in both the *TRACE* and modeled loops is rightward-directed. According to Martin et al. (1994), this

<sup>5</sup> Based upon this, we estimate the density of electric currents in the postflare loops: the extrapolated magnetic field strength is about 300 G, which implies current density of  $0.006 \text{ A m}^{-2}$ .

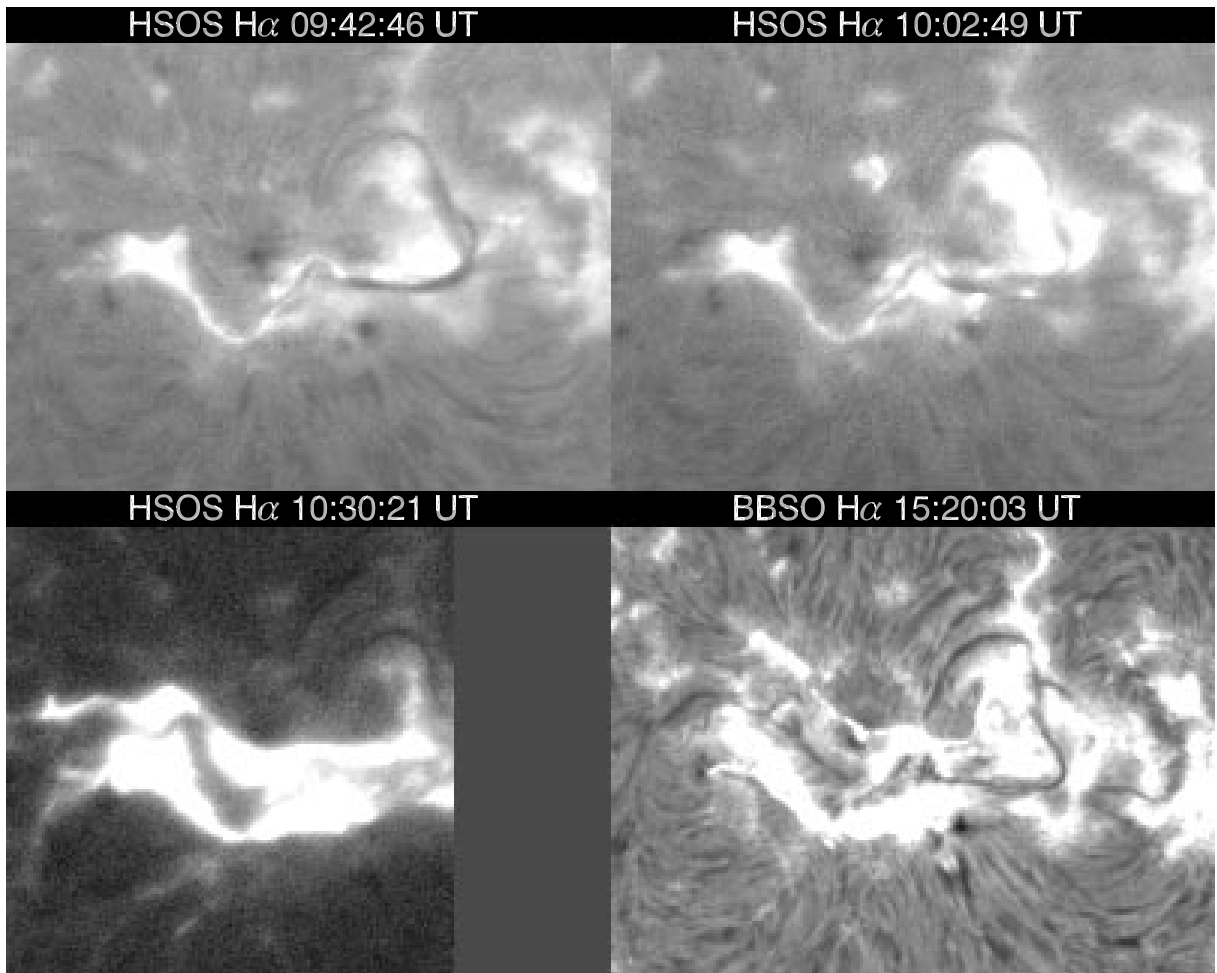


FIG. 6.—HSOS and BBSO  $H\alpha$  observations of a two-ribbon flare on 2000 July 14. North is to the top, west is to the right.

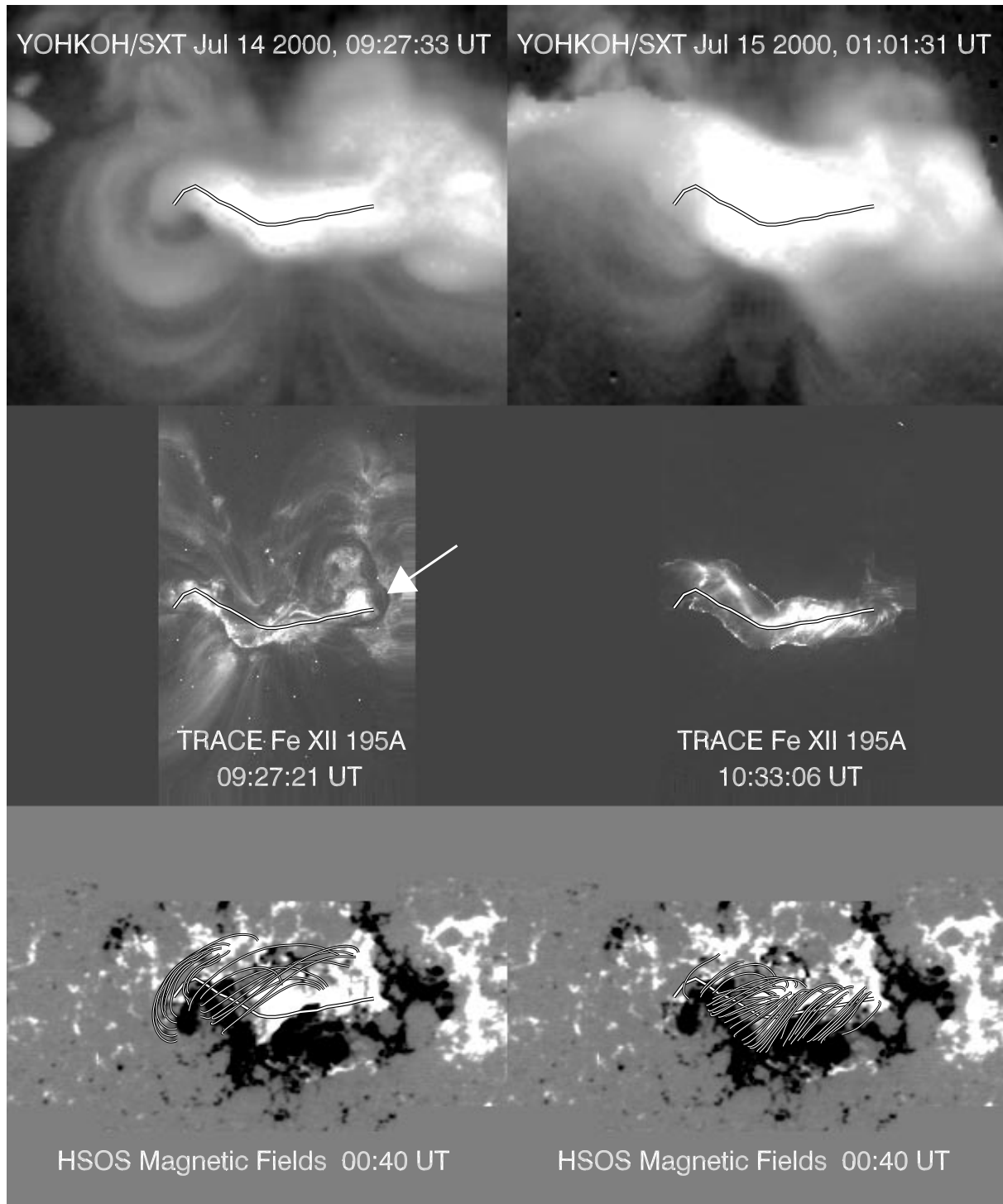


FIG. 7.—*Yohkoh* and *TRACE* pre- and postflare images of a 2000 July 14 two-ribbon flare. *Bottom*: HSOS longitudinal field overlaid with linear force-free field lines. North is to the top, west is to the right.

implies that the postflare system is dextral or has negative helicity. It is uncertain from the  $H\alpha$  images (Fig. 6) whether sunspots were twisted clockwise or counterclockwise. However, the large X-ray loop was reverse-S-shaped, which suggests negative magnetic helicity. In the HSOS magnetogram, we indicate the location of the large X-ray loop seen before eruption with a thick white curve. The comparison of the *Yohkoh*/SXT image and HSOS magnetogram shows that the axial field in the large X-ray loop was

west-east-directed, which coincides with the model calculations.

The eruption and the two-ribbon flare were followed by a halo CME (Fig. 8). The July 14 CME was extremely fast: its mean velocity was about  $1500 \text{ km s}^{-1}$ , and according to SOHO/CELIAS/MTOF Proton Monitor<sup>6</sup> its arrival was preceded by a strong interplanetary shock (see also Klein &

<sup>6</sup> Available at <http://sohowww.nascom.nasa.gov/data/CME/20000714>.

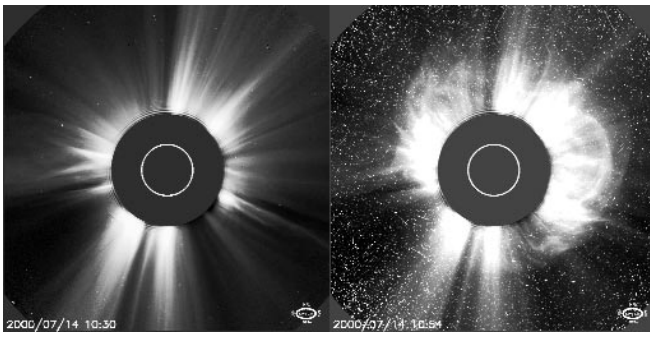


FIG. 8.—LASCO C2 images at 10:39 UT (left) and 10:54 UT (right), showing the halo CME on 2000 July 14.

Burlaga 1982; Vandas et al. 1997). The CME arrival was also accompanied by a severe magnetic storm, during which the Dst index decreased to  $-300$  (see Fig. 9, bottom panel). The figure also plots 1 hr averages of the IMF at about 0.99 AU from the Sun. An MC is identified by the rapid growth of the magnetic field on July 15 at about 14:00 UT. The orientation of the magnetic field in the July 15 MC was quite different from what we found in the previous case (Fig. 4). At the moment of the MC arrival,  $t_1$ , the  $B_z$  component was directed southward, and it rotated during the passage of the satellite through the MC (Fig. 9; X-Z plot). At the same time, the signs of the  $B_x$  and  $B_y$  components did not change (Y-Z and X-Y plots). The fact that the  $B_z$  component rotates implies that it is the azimuthal component of the flux rope's magnetic field and that the axis of the flux rope is oriented in the east-west direction. The  $B_z$  component vanishes on July 16, at  $t_2 \approx 00:00$  UT, which suggests that the axis of the flux tube is nearly in the plane of the ecliptic, i.e., it runs nearly along the Sun's equator (note that, on 2000 July 14,  $P_0 = 3^\circ$ ). From Figure 10, we also conclude that the direction of the axial magnetic field and

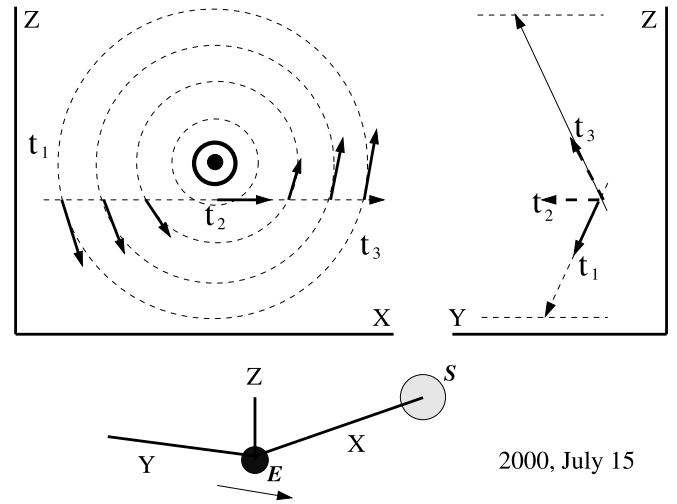


FIG. 10.—Cartoon showing the orientation of the flux rope in the July 15 MC. Coordinate system is GSE.

its helicity in the July 15 MC coincide with the direction and helicity of the large X-ray loop and of the entire active region as well.

5. CONCLUSIONS AND DISCUSSION

Geomagnetic storms are a sustained response of the Earth's magnetosphere to a prolonged action of a strong, southward-directed interplanetary field. When reconnection occurs between the southward-directed interplanetary magnetic field and the Earth's northward-directed magnetic field, additional ions arrive in the ring current from the plasma sheet, causing a dramatic increase in the current and significant distortion of the Earth's magnetic field.

Figure 11 shows the orientations of the active regions, the MCs, and Earth's magnetic fields. In the case of the February 17 CME (top two panels), the magnetic field in the flux rope is northward-oriented, and it has positive helicity, consistent with the helicity of the magnetic field in the active region (see also Figs. 1 and 4). The axial magnetic field in the MC is estimated to be nearly parallel to the Earth's magnetic field and to the active region magnetic fields as well. There is no southward component in the MC and, consequently, no geomagnetic activity was associated with the CME. For CMEs with the north-south-oriented axial magnetic fields, their geoeffectiveness is largely defined by the direction of the axial field, and the sign of helicity plays a minor role.

For the July 14 CME, the axial magnetic field was directed eastward (see also Figs. 7 and 9). The azimuthal component in the MC was southward-directed, which assumes a strong geomagnetic activity following the CME's arrival. For a CME with the east-west-oriented axial field, only the sign of the magnetic helicity defines the direction of the azimuthal field (which is nearly north-south-oriented) and the geoeffectiveness of a given CME.

In both cases analyzed here, the directions of the helical magnetic fields in the leading edge of the magnetic clouds were consistent with the direction and helicity of the magnetic fields overlying the active region filaments (Bothmer & Schwenn 1994; Rust 1994; Marubashi 1997).

Our study shows that an Earth-directed CME may or may not be associated with a geomagnetic storm. In the general case, it depends on the orientation of the magnetic

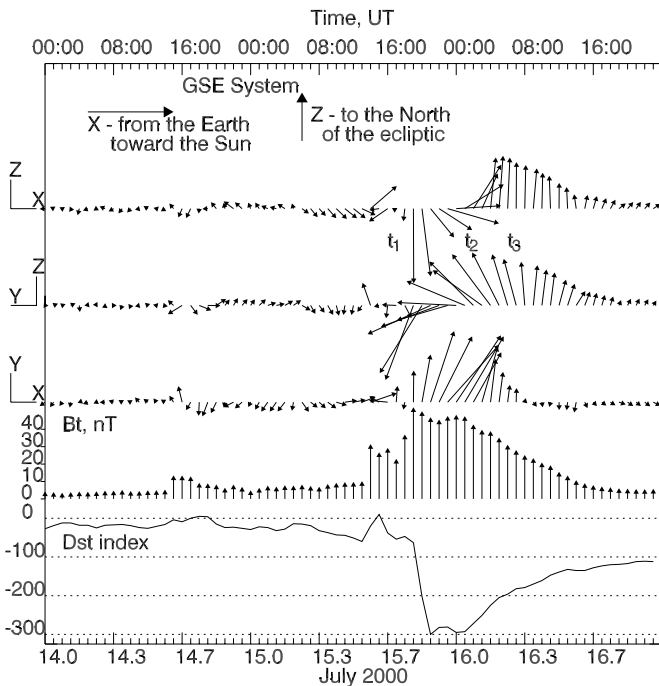


FIG. 9.—Same as Fig. 4, but for the IMF in the 2000 July 15 MC

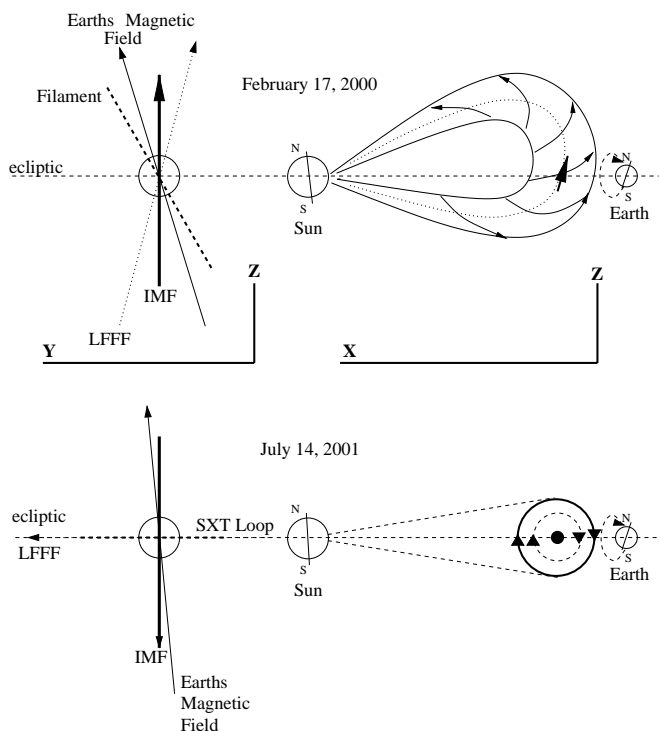


FIG. 11.—Cartoon of two CME/MC events: 2000 February 17 (*top*) and 2000 July 15 (*bottom*). *Left*: Directions of overlaying linear force-free fields, filaments, and IMFs; *right*: inferred structure of the MCs and orientation of the Earth's magnetic field.

field in an active region and the sign of the magnetic helicity. We have shown that, by using combined space- and ground-based observations, we can predict the orientation of a magnetic cloud associated with a CME and, furthermore, the likelihood of geomagnetic storms. The key is to establish if there is a southward component in the projected MC. Filament chirality and/or the sign of the active region's helicity may be defined in a number of ways, which are mentioned in § 3.

There are at least two different approaches to explain the origin of a CME (see Krall, Chen, & Santoro 2000 for review). One suggests that a twisted flux rope is formed long before the eruption in the magnetic field (Chen et al. 1997; Chen 2001), while the other advocates the idea that magnetic reconnection of erupting sheared arcades results in the formation of a flux rope (Gosling 1993; Low 1977; Mikić, Barnes, & Schnack 1988; Dere et al. 1999). Here we would like to note that the first idea is usually supported by the fact that flux rope eruptions indeed takes place in the solar photosphere (Tanaka 1991; Leka et al. 1996). However, flux emergence occurs everywhere in an evolving active region, while flux rope eruptions and CMEs are largely associated with the active region's major neutral line. Our study suggests that both scenarios may be equally likely. We believe that the February 17 CME originated by reconnection of the sheared arcades seen in the *Yohkoh* images and in the model calculations. To the contrary, there is a little doubt that the large X-ray loop seen in the July 14 *Yohkoh* image was a superposition of two or more sheared arcades. In the preflare 09:27 UT *TRACE* image, we do not see any signs of these arcades, although we clearly can distinguish the footpoints of the ring-shaped SXT loops, which are located very close to the neutral line. The combination of the preflare *Yohkoh* and *TRACE* data suggests that the July 14 CME was a result of the eruption of the preexisting large X-ray loop. The filament eruption described in Zhang et al. (2001), may be the trigger that forced the large X-ray loop to erupt. It is interesting to note the results of Yan et al. (2001), who claim that a preexisting flux rope could be sitting along the neutral line under the overlying field. If that were the case, the flux rope may lose its balance and trigger the eruption of the large X-ray loop.

We thank anonymous referee for valuable remarks and suggestions that resulted in improvement of the paper. This work was supported in part by ATM 00-76602, ATM 99-03515 and NASA (NAG 5-9682) grants. *SOHO* is a project of international cooperation between ESA and NASA.

#### REFERENCES

- Abramenko, V. I., Wang, T., & Yurchishin, V. B. 1996, *Sol. Phys.*, 168, 75  
 Abramenko, V. I., & Yurchishin, V. B. 1996, *Sol. Phys.*, 168, 47  
 Amari, T., Luciani, J. F., Mikić, Z., & Linker, J. 2000, *ApJ*, 529, L49  
 Bothmer, V., & Schwenn, R. 1994, *Space Sci. Rev.*, 70, 215  
 Burlaga, L. F. 1988, *J. Geophys. Res.*, 93, 7217  
 Burlaga, L. F., Sittler, E., Mariani, F., & Schwenn, R. 1981, *J. Geophys. Res.*, 86, 6673  
 Canfield, R. C., Hudson, H. S., & McKenzie, D. E. 1999, *Geophys. Res. Lett.*, 26, 627  
 Chen, J. 2001, *Space Sci. Rev.*, 95, 165  
 Chen, J., et al. 1997, *ApJ*, 490, L191  
 Dere, K. P., Brueckner, G. E., Howard, R. A., Michels, D. J., & Delaboudinière, J.-P. 1999, *ApJ*, 516, 465  
 Gosling, J. T. 1993, *J. Geophys. Res.*, 98, 18937  
 Hale, G. E. 1927, *Nature*, 119, 708  
 Klein, L. W., & Burlaga, L. F. 1982, *J. Geophys. Res.*, 87, 613  
 Kosovichev, A. G., & Zharkova, V. V. 2001, *ApJ*, 550, L105  
 Krall, J., Chen, J., & Santoro, R. 2000, *ApJ*, 539, 964  
 Leka, K. D., Canfield, R. C., McClymont, A. N., & van Driel-Gesztelyi, L. 1996, *ApJ*, 462, 547  
 Low, B. C. 1977, *ApJ*, 212, 234  
 Martin, S. F., Billimoria, R., & Tracadas, P. W. 1994, in *Solar Surface Magnetism*, ed. R. J. Rutten & C. J. Schrijver (ASI Ser. C, 433; Dordrecht: Kluwer), 303  
 Marubashi, K. 1997, in *Geophys. Monogr. Ser. 99, Coronal Mass Ejections*, ed. N. Crooker, J. A. Joselyn, & J. Feynman (Washington: AGU), 147  
 Matsumoto, R., Tajima, T., Shibata, K., & Kaisig, M. 1993, *ApJ*, 414, 357  
 McAllister, H., & Martin, S. F. 2000, *Adv. Space Res.*, 26, 469  
 Mikić, Z., Barnes, D. C., & Schnack, D. D. 1988, *ApJ*, 328, 830  
 Mouradian, Z., Soru-Escout, I., & Pojoga, S. 1995, *Sol. Phys.*, 158, 269  
 Nakagawa, Y., Raadu, M. A., Billings, D. E., & McNamara, D. 1971, *Sol. Phys.*, 19, 72  
 Pevtsov, A. A., Canfield, R. C., & Metcalf, T. R. 1995, *ApJ*, 440, L109  
 Richardson, R. S. 1941, *ApJ*, 93, 24  
 Rust, D. M. 1994, *Geophys. Res. Lett.*, 21, 241  
 Rust, D. M., & Kumar, A. 1996, *ApJ*, 464, L199  
 Rust, D. M., & Martin, S. F. 1994, in *ASP Conf. Ser. 68, Solar Active Region Evolution: Comparing Models with Observations*, ed. K. S. Balasubramanian & G. W. Simon (San Francisco: ASP), 337  
 Seehafer, N. 1990, *Sol. Phys.*, 125, 219  
 Smith, S. F. 1968, in *IAU Symp. 35, Structure and Development of Solar Active Regions*, ed. K. O. Kiepenheuer (Dordrecht: Reidel), 267  
 Tanaka, K. 1991, *Sol. Phys.*, 136, 133  
 Vandas, M., Fischer, S., Dryer, D., Smith, Z., Detman, T., & Geranios, A. 1997, *J. Geophys. Res.*, 102, 22295  
 Wang, H., Chae, J., Yurchyshyn, V. B., Yang, G., Steinegger, M., & Goode, P. R. 2001, *ApJ*, 559, 1171  
 Webb, D. F. 1992, in *Eruptive Solar Flares*, ed. Z. Svestka, B. V. Jackson, & M. E. Machado (New York: Springer), 234  
 Wilson, R. M., & Hildner, E. 1984, *Sol. Phys.*, 91, 169  
 Yan, Y., Deng, Y., Karlický, M., Fu, Q., Wang, S., & Liu, Y. 2001, *ApJ*, 551, L115  
 Zhang, J., Wang, J., Deng, Y., & Wu, D. 2001, *ApJ*, 548, L99  
 Zirker, J. B., Martin, S. F., Harvey, K., & Gaizauskas, V. 1997, *Sol. Phys.*, 175, 27